Biochimie 200 (2022) 172–183

Contents lists available at ScienceDirect

Biochimie

journal homepage: www.elsevier.com/locate/biochi

Stbd1-deficient mice display insulin resistance associated with enhanced hepatic ER-mitochondria contact

Styliana Kyriakoudi [a], Andria Theodoulou [a], Louiza Potamiti [b], Fabian Schumacher [c], Margarita Zachariou [d], Revekka Papacharalambous [e], Burkhard Kleuser [c], Mihalis I. Panayiotidis [b], Anthi Drousiotou [a], Petros P. Petrou [a, *]

[a] Biochemical Genetics Department, The Cyprus Institute of Neurology and Genetics, P.O. Box 23462, 1683, Nicosia, Cyprus
[b] Cancer Genetics, Therapeutics & Ultrastructural Pathology Department, The Cyprus Institute of Neurology and Genetics, P.O. Box 23462, 1683, Nicosia, Cyprus
[c] Freie Universität Berlin, Institute of Pharmacy, Königin-Luise-Str. 2+4, Berlin, Germany
[d] Bioinformatics Department, The Cyprus Institute of Neurology and Genetics, P.O. Box 23462, 1683, Nicosia, Cyprus
[e] Neuropathology Lab, Center for Neuromuscular Disorders, The Cyprus Institute of Neurology and Generics, P.O. Box 23462, 1683, Nicosia, Cyprus

ARTICLE INFO

Article history:
Received 25 January 2022
Received in revised form
19 May 2022
Accepted 7 June 2022
Available online 9 June 2022

Keywords:
STBD1
Insulin resistance
Glycogen
Mitochondria-ER Contact sites
Mitochondrial fragmentation
Mice

ABSTRACT

Starch binding domain-containing protein 1 (STBD1) is an endoplasmic reticulum (ER)-resident, glycogen-binding protein. In addition to glycogen, STBD1 has been shown to interact with several proteins implicated in glycogen synthesis and degradation, yet its function in glycogen metabolism remains largely unknown. In addition to the bulk of the ER, STBD1 has been reported to localize at regions of physical contact between mitochondria and the ER, known as Mitochondria-ER Contact sites (MERCs). Given the emerging correlation between distortions in the integrity of hepatic MERCs and insulin resistance, our study aimed to delineate the role of STBD1 *in vivo* by addressing potential abnormalities in glucose metabolism and ER-mitochondria communication associated with insulin resistance in mice with targeted inactivation of *Stbd1* (*Stbd1*KO). We show that *Stbd1*KO mice at the age of 24 weeks displayed reduced hepatic glycogen content and aberrant control of glucose homeostasis, compatible with insulin resistance. In line with the above, *Stbd1*-deficient mice presented with increased fasting blood glucose and insulin levels, attenuated activation of insulin signaling in the liver and skeletal muscle and elevated liver sphingomyelin content, in the absence of hepatic steatosis. Furthermore, *Stbd1*KO mice were found to exhibit enhanced ER-mitochondria association and increased mitochondrial fragmentation in the liver. Nevertheless, the enzymatic activity of hepatic respiratory chain complexes and ER stress levels in the liver were not altered. Our findings identify a novel important role for STBD1 in the control of glucose metabolism, associated with the integrity of hepatic MERCs.

1. Introduction

Energy homeostasis and metabolic activity are largely regulated by insulin. In the liver, insulin stimulates glycogen synthesis, promotes lipogenesis and suppresses gluconeogenesis [1]. An impaired responsiveness of tissues to insulin is described as insulin resistance and is a cardinal feature and a major contributor to the pathophysiology of type 2 diabetes (T2D). During insulin resistance, hepatic glucose production is inefficiently suppressed and at the same time glucose uptake by peripheral tissues such as the skeletal muscle and adipocytes is compromised [1]. To counteract this imbalance, insulin production by pancreatic β-cells is upregulated, hence insulin resistance is often accompanied by hyperglycemia and hyperinsulinemia [2].

The understanding of the molecular mechanisms underlying insulin resistance is essential for the development of effective therapeutic approaches to treat T2D. Genetic association studies in humans [3,4] in addition to data from knockout and transgenic mice [5] identified a plethora of genes and loci implicated in the

Abbreviations: ER, Endoplasmic reticulum; FOXO1, Forkhead box protein O1; G6PC, Glucose-6-phosphatase; MERCs, Mitochondria-ER Contact sites; OXPHOS, Oxidative phosphorylation; PEPCK, Phosphoenolpyruvate carboxykinase; STBD1, Starch binding domain-containing protein 1; T2D, Type 2 diabetes.

* Corresponding author. Department of Biochemical Genetics, The Cyprus Institute of Neurology and Genetics, 6 Iroon avenue, Agios Dometios, 2371, Nicosia, Cyprus.
E-mail address: petrosp@cing.ac.cy (P.P. Petrou).

https://doi.org/10.1016/j.biochi.2022.06.003

development of insulin resistance, highlighting the complexity of the factors and processes contributing to this condition. Among these, are proteins involved in the physical association and communication between the endoplasmic reticulum (ER) and mitochondria [6,7]. The cross-talk between the two organelles occurs through dynamic regions of close apposition between them, known as Mitochondria-ER Contact sites (MERCs). MERCs are implicated in different cellular processes such as the transfer of phospholipids and calcium between the ER and mitochondria, the regulation of mitochondrial dynamics, ER stress and inflammation [8]. Over the past years, MERCs have been further recognized as important hubs of insulin signaling whereas distortions in ER-mitochondria communication have been linked to insulin resistance [9,10].

We have previously reported that the glycogen-binding protein Starch binding domain-containing protein 1 (STBD1) is a transmembrane, ER-resident protein that is also found at MERCs in HeLa cells [11]. The presence of STBD1 at MERCs is further supported by proteomic studies on mitochondria-associated membrane preparations from rabbit skeletal muscle as well as mouse liver and brain [12,13]. Recently, a link between STBD1 and ER stress has been established. STBD1 was identified as a downstream target of the ER stress response in mouse myoblasts specifically promoting the formation of ER-associated glycogen clusters in response to ER stress activation [14].

The reported correlation between STBD1 with MERCs and ER stress and their implication in insulin resistance prompted us to address the question whether STBD1 deficiency is associated with distortions in glucose metabolism. In the present study we demonstrate that *Stbd1* knockout (*Stbd1*KO) mice display metabolic abnormalities compatible with insulin resistance. These include increased levels of blood insulin, reduced liver glycogen content, attenuated response to insulin and enhanced gluconeogenesis. Moreover, the above metabolic distortions were associated with alterations in hepatic MERCs and mitochondrial dynamics without any obvious impact on respiratory chain enzyme activities.

Our findings identify a novel role for STBD1 in glucose homeostasis and support the correlation between insulin resistance and enhanced ER-mitochondria cross-talk.

2. Materials and methods

2.1. Animals

*Stbd1*KO mice were obtained from the Canadian Mouse Mutant Repository. The mouse line C57BL/6N-Stbd1<tm1b (KOMP)Wtsi>/Tcp was made as part of the KOMP2-DTCC project with C57BL/6NStbd1<tm1a (KOMP)Wtsi>/Tcp made from KOMP ES cells at the Toronto Centre for Phenogenomics [15]. *Stbd1*KO and wild type control mice were obtained from heterozygous $Stbd1^{+/-}$ intercrosses and maintained on a C57BL6 background. The genotype of the animals was determined by multiplex PCR using the KAPA HotStart® mouse genotyping kit (KAPA Biosystems) and primers specific for the wild type and targeted allele (Supplementary Table 1). All animals were housed under temperature- and humidity-controlled conditions with 12 h light/12 h dark cycle and provided free access to standard chow diet (Mucedola, 4RF25: 70% of energy as carbohydrate, 20% protein and 10% fat) and water, unless otherwise stated. The experimental procedures described in this study were performed on 24-week-old male *Stbd1*KO and wild type control mice in agreement with animal care protocols approved by the Cyprus Government's Chief Veterinary Officer (Project licence CY/EXP/PR.L11/2019) and according to EU guidelines (EC Directive 86/609/EEC).

2.2. Glucose, insulin and pyruvate loading tests

For the glucose tolerance test, mice were administered 2 g glucose/kg bodyweight (BW) using an oral gavage, following a 6-h fast. For the insulin tolerance test, 0.75 units insulin/kg BW (HumulinR, Lilly) were injected intraperitoneally in 4-h fasted mice. For the pyruvate loading test, 2 g sodium pyruvate/kg BW were intraperitoneally administrated in 6-h fasted mice. In all three tests, baseline glucose was determined prior to glucose, insulin or sodium pyruvate administration, using an *Accu*-Chek® Guide glucose meter in blood samples collected by tail tip clipping. Blood glucose levels (mg/dL) were determined at 15, 30, 45, 60, 90 and 120 min after substance administration. The area under the curve (AUC) for each individual animal was calculated, using the *auc* function from the MESS package (Miscellaneous Esoteric Statistical Scripts by Claus Thorn Ekstrøm (2020), R package version 0.5.7) in *R 4.1.0* (Core Team (2021). R: A language and environment for statistical computing. R Foundation for Statistical Computing, Vienna, Austria). For the area calculation the spline interpolation option was selected for which the *auc* function uses the *splinefun* and *integrate* functions to calculate the numerical integral.

2.3. Quantification of glycogen

Quantification of glycogen was performed in the gastrocnemius muscle of randomly fed mice and in liver tissue either at randomly fed conditions, upon 18 h of fasting or at 3 h after refeeding following an 18-h fast. Tissues (20–30 mg) were boiled in 300 μl 30% KOH solution until completely lysed and 100 μl of 1 M Na_2SO_4 were added to the homogenate after cooling. Precipitation of glycogen was achieved by adding 800 μl ethanol followed by centrifugation at 10,000 *g* for 5 min and the resulting pellet was resuspended in 200 μl 0.2 M sodium acetate pH 4.6. Glycogen was enzymatically degraded by adding 1.5 μl amyloglucosidase solution (30 mg/mL) from *Aspergillus niger*. Liberated glucose was determined by a colorimetric assay using the glucose oxidase/peroxidase system and 2,2′-azino-bis-3-ethylbenzothiazoline-6-sulfonic acid (ABTS) as substrate. Absorbance at 405 nm was measured with a Synergy H1 microplate reader (BioTek). Glycogen concentration was expressed as μg glucose/mg tissue.

2.4. Measurement of serum insulin levels

Serum insulin levels were quantitatively determined using an Enzyme-Linked Immunosorbent Assay (ELISA) kit (CrystalChem) in blood samples taken from mouse tail tips after 6 h of fasting and at 1 h after refeeding, following a 6-h morning fast. Measurement was performed using 5 μl of serum according to the instructions of the manufacturer. Absorbance was measured using a microplate reader (BioTek) and insulin concentration was calculated in ng/mL based on a standard curve.

2.5. Quantification of liver triglycerides

Quantitative determination of liver triglycerides was performed as described in Ref. [16]. Briefly, liver tissue (200–300 mg) was digested in 350 μl ethanolic KOH (2 parts ethanol: 1 part 30% KOH) for 16 h at 55 °C. Following centrifugation at 8000 *g* for 5 min, the supernatant was topped up to 1200 μl with H_2O: EtOH (1:1) with sequential addition of 1300 μl 1 M $MgCl_2$ and left on ice for 10 min. Next, 6 μl of the supernatant were mixed with 200 μl of free glycerol reagent (Sigma) and absorbance at 540 nm was measured after 15 min on a microplate reader (BioTek). The concentration was calculated based on a standard curve created with glycerol (Sigma) and expressed as μg triglycerides/mg tissue.

2.6. Sphingolipid and diacylglycerol quantification by LC-MS/MS

Liver tissue homogenates were subjected to lipid extraction using 1.5 mL methanol/chloroform (2:1, v:v) as described in Refs. [17,18]. The extraction solvent contained either ceramide d18:1/17:0 (C17 Cer) and sphingomyelin d18:1/16:0-d_{31} (C16-d_{31} SM), or 1,3-diheptadecanoin-d_5 (C17/C17-d_5 DAG) as internal standards (Avanti Polar Lipids, Alabaster, USA). Details of ceramide (Cer), sphingomyelin (SM), and diacylglycerol (DAG) analysis by LC-MS/MS have been described elsewhere [17,19]. Briefly, chromatographic separations were performed on a 1290 Infinity II HPLC (Agilent Technologies, Waldbronn, Germany) equipped with a Poroshell 120 EC-C8 column (3.0 × 150 mm, 2.7 μm; Agilent Technologies). MS/MS analyses were carried out using either an Agilent 6495C TQ-MS (DAG analysis) or an Agilent Ultivo TQ-MS (Cer and SM analysis) operating in positive electrospray ionization mode (ESI+). The following mass transitions were recorded (qualifier product ions in parentheses), ceramides: *m/z* 520.5 → 264.3 (282.3) for C16 Cer, *m/z* 534.5 → 264.3 (282.3) for C17 Cer, *m/z* 548.5 → 264.3 (282.3) for C18 Cer, *m/z* 576.6 → 264.3 (282.3) for C20 Cer, *m/z* 604.6 → 264.3 (282.3) for C22 Cer, *m/z* 630.6 → 264.3 (282.3) for C24:1 Cer, and *m/z* 632.6 → 264.3 (282.3) for C24 Cer; sphingomyelins: *m/z* 703.6 → 184.1 (86.1) for C16 SM, *m/z* 731.6 → 184.1 (86.1) for C18 SM, *m/z* 734.6 → 184.1 (86.1) for C16-d_{31} SM, *m/z* 759.6 → 184.1 (86.1) for C20 SM, *m/z* 787.7 → 184.1 (86.1) for C22 SM, *m/z* 813.7 → 184.1 (86.1) for C24:1 SM, and *m/z* 815.7 → 184.1 (86.1) for C24 SM; diacylglycerols: *m/z* 551.5 → 57.2 (239.2) for C16/C16 DAG, *m/z* 579.5 → 239.2 (267.3) for C16/C18 DAG, *m/z* 584.6 → 57.2 (253.2) for C17/C17-d_5 DAG, *m/z* 607.6 → 57.2 (267.3) for C18/C18 DAG, *m/z* 612.6 → 313.3 (339.3) for C16/C18:1 DAG, and *m/z* 662.6 → 341.3 (361.3) for C18/C20:4 DAG. Peak areas of Cer, SM and DAG subspecies, as determined with MassHunter software (Agilent Technologies), were normalized to those of corresponding internal standards (C17 Cer, C16-d_{31} SM and C17/C17-d_5 DAG, respectively) followed by external calibration in the range of 1 fmol–50 pmol on column. Determined lipid amounts were normalized to the weight of the tissue [mg] used for extraction.

2.7. Oil Red O staining

Paraformaldehyde-fixed liver sections were incubated in 60% isopropanol for 5 min, followed by a 10-min incubation in 0.5% Oil Red O/isopropanol stain. The tissues were washed briefly in 60% isopropanol, rinsed in distilled water and counterstained with hematoxylin for 5 s. Sections were subsequently rinsed with distilled water and mounted in Kaiser's glycerol gelatine (Merck). Images were captured using an IX73P1F inverted microscope (Olympus).

2.8. Immunoblot analysis

Liver tissue and gastrocnemius muscle were isolated from 6-h fasted mice, intraperitoneally injected with either insulin (2 units/kg BW) or saline, 5 and 20 min after the injection, respectively. Relative protein levels of OXPHOS complexes were assessed in liver lysates from randomly fed mice. Tissue homogenates were prepared in lysis buffer (50 mM Tris-HCl, pH 7.4, 150 mM NaCl, 1% NP-40, 0.5% sodium deoxycholate, 0.1% SDS), supplemented with protease and phosphatase inhibitors (Cell Signaling), using an all-glass homogenizer. Tissue lysates were subsequently subjected to sonication and centrifugation at 10,000 *g* for 20 min at 4 °C. Protein concentration was determined in the supernatant using the Bicinchoninic Acid (BCA) protein assay [20]. Total tissue protein (70 μg) was resolved by *SDS-PAGE,* transferred to PVDF membranes (GE Healthcare, Life Sciences) and incubated with primary antibodies overnight. Membranes were probed with Horseradish peroxidase–conjugated anti-mouse or anti-rabbit secondary antibodies (Cell Signaling) and visualized using the Clarity Western ECL substrate (BioRad) and a Vilber FUSION Solo 6X imager. Densitometry analysis was performed using ImageJ. The following primary antibodies were used: AKT (4685, Cell Signaling); phospho AKT (Ser473) (4060, Cell Signaling), FOXO1 (L27) (9454, Cell Signaling); phospho FOXO1 (Ser256) (9461, Cell Signaling); total OXPHOS rodent WB Antibody Cocktail (ab110413, Abcam) and GAPDH (sc-32233, Santa Cruz).

2.9. Transmission electron microscopy and quantification of ER-mitochondria contacts

Liver tissues from randomly fed mice were fixed in 2.5% glutaraldehyde and osmium, washed in 0.1 M phosphate buffer pH 7.2, dehydrated in a series of graded ethanol and embedded in an epon and araldite resin mixture (Agar Scientific). Ultrathin sections of 0.1 μm were prepared on a Reichert-Jung UCT ultramicrotome (Leica), mounted on 300-mesh copper grids and stained with uranyl acetate and lead citrate. Liver sections were observed on a JEM 1010 transmission electron microscope (JEOL) and images collected using a Mega View G2 digital camera (Olympus). MERCs were quantified by measuring the length of the contact region between the ER and mitochondria, and expressed as a percentage of the mitochondrial perimeter. Mitochondrial morphology parameters including perimeter (μm), area (μm^2), circularity and aspect ratio were calculated by tracing the outer membrane of each mitochondrion and using the ROI manager tool of the ImageJ software as described in Ref. [21].

2.10. Measurement of the enzymatic activity of mitochondrial respiratory chain complexes

Liver tissue was homogenized in lysis buffer (250 mM sucrose, 2 mM EDTA, 100 mM Tris-HCl, pH 7.45) using an all-glass homogenizer and cleared by centrifugation at 600*g* for 20 min. The supernatant was used to measure the activity of the following respiratory chain enzymes in a temperature-controlled spectrophotometer at 30 °C, as described in Ref. [22]: NADH dehydrogenase (Complex I), succinate dehydrogenase (Complex II), NADH cytochrome C reductase-total and rotenone sensitive/resistant (Complex I + III), succinate cytochrome C reductase (Complex II + III) and Cytochrome C oxidase (Complex IV). Values were normalized to the activity of citrate synthase. Enzymatic activities were expressed as μmol/min/g tissue.

2.11. RNA isolation, reverse transcription and qPCR

Total RNA was isolated from liver tissue using the RNAzol RT reagent (Sigma) and cDNA synthesis was performed with the PrimeScript RT Reagent Kit (Perfect Real Time; TaKaRa Bio), following the manufacturer's instructions. Quantitative real-time PCR was performed on an Applied Biosystems 7900HT real-time PCR system using the KAPA SYBR FAST qPCR Master Mix (KAPA Biosystems). *Actb* (β-actin) was used as housekeeping gene. Data were analyzed using LinRegPCR version 2020.0 [23].

2.12. Statistical analysis

All statistical comparisons were performed using a two-tailed unpaired Student's *t*-test and the GraphPad Prism 8 software. Data are presented as mean ± SEM and statistical significance was assumed at $P \leq 0.05$.

3. Results

3.1. Stbd1KO mice display reduced liver glycogen content

For the purposes of this study, *Stbd1*KO and wild type male mice at the age of 24 weeks were employed. *Stbd1*KO mice on a C57Bl6 background are fertile and superficially unremarkable in appearance. RT-PCR verified the lack of *Stbd1* transcripts in *Stbd1*KO mice and the expression of the *LacZ* reporter gene that was included in the targeting vector (Fig. S1A). *Stbd1* inactivation was further confirmed by quantitative PCR (Fig. S1B).

*Stbd1*KO mice showed similar weight gain to wild type controls, monitored over a period of 20 weeks starting at weaning, at the age of 4 weeks (Fig. 1A). STBD1 has been previously reported to bind glycogen through its carboxyterminal CBM20 domain and interact with several proteins implicated in glycogen metabolism [24,25]. Given the above, we evaluated the levels of glycogen in the liver and skeletal muscle of *Stbd1*KO as compared to wild type control mice. We found that randomly fed *Stbd1*KO mice displayed significantly reduced liver glycogen (Fig. 1B). Moreover, an 18-h fasting period resulted in the near complete depletion of liver glycogen stores in *Stbd1*KO mice as opposed to wild type animals, which exhibited significantly higher hepatic glycogen levels (Fig. 1B). Notably, liver glycogen content was found to be similar in both wild type and *Stbd1*KO mice 3 h after refeeding following an 18-h fast, suggesting that replenishment of liver glycogen stores after fasting is comparable between the two genotypes (Fig. 1B). In contrast to the liver, both genotypes featured comparable glycogen content in skeletal muscle at fed conditions (Fig. 1C).

3.2. STBD1 deficiency causes insulin resistance and associated distortions in the control of glucose homeostasis

The reduced hepatic glycogen content under randomly fed and fasting conditions may suggest that *Stbd1*KO mice display distortions in the control of glucose homeostasis. To address the above, we initially monitored blood glucose levels at different feeding conditions. *Stbd1*KO and wild type control mice displayed

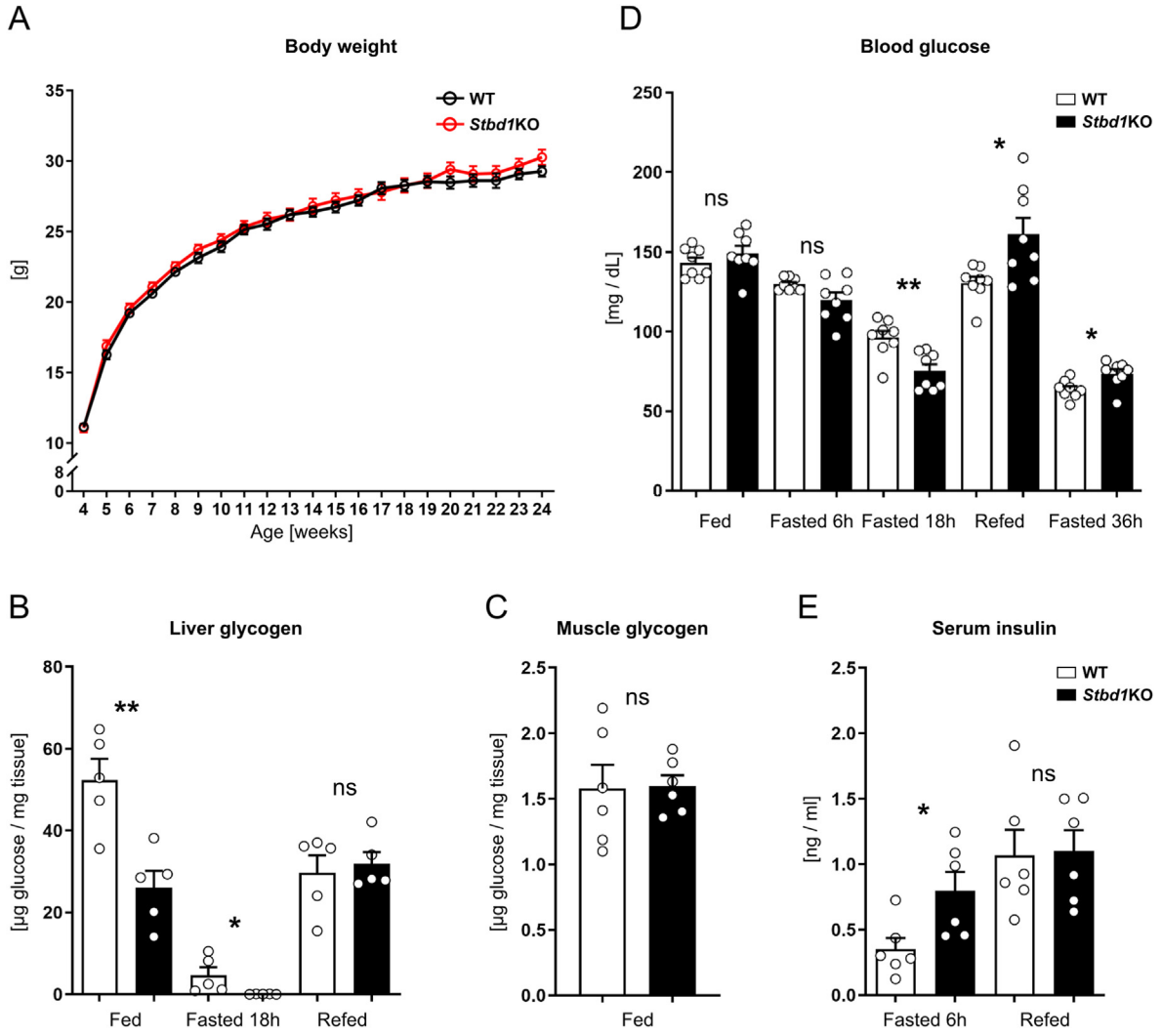

Fig. 1. *Stbd1*KO mice display reduced hepatic glycogen content, increased serum insulin and dysregulated blood glucose control
(A) The body weight of *Stbd1*KO and wild type mice (n = 15 per genotype) was monitored for 20 weeks, starting at weaning at the age of 4 weeks. (B) Quantitative determination of hepatic glycogen levels in randomly fed mice, at 18 h of fasting and at 3 h after refeeding following an 18-h fast (n = 5 per group). (C) Quantitative determination of glycogen levels in the gastrocnemius muscle of randomly fed *Stbd1*KO and wild type mice (n = 6 per genotype). (D) Blood glucose measurements at fed conditions, at 6 h, 18 h and 36 h of fasting and at 3 h after refeeding following an 18-h fast (n = 8 per group) (E). Quantification of serum insulin levels at 6 h of fasting and 1 h after refeeding following a 6-h fast, by means of ELISA (n = 6 per group). Values are expressed as mean ± SEM, *P < 0.05, **P < 0.01, ns, not significant (unpaired Student's *t*-test).

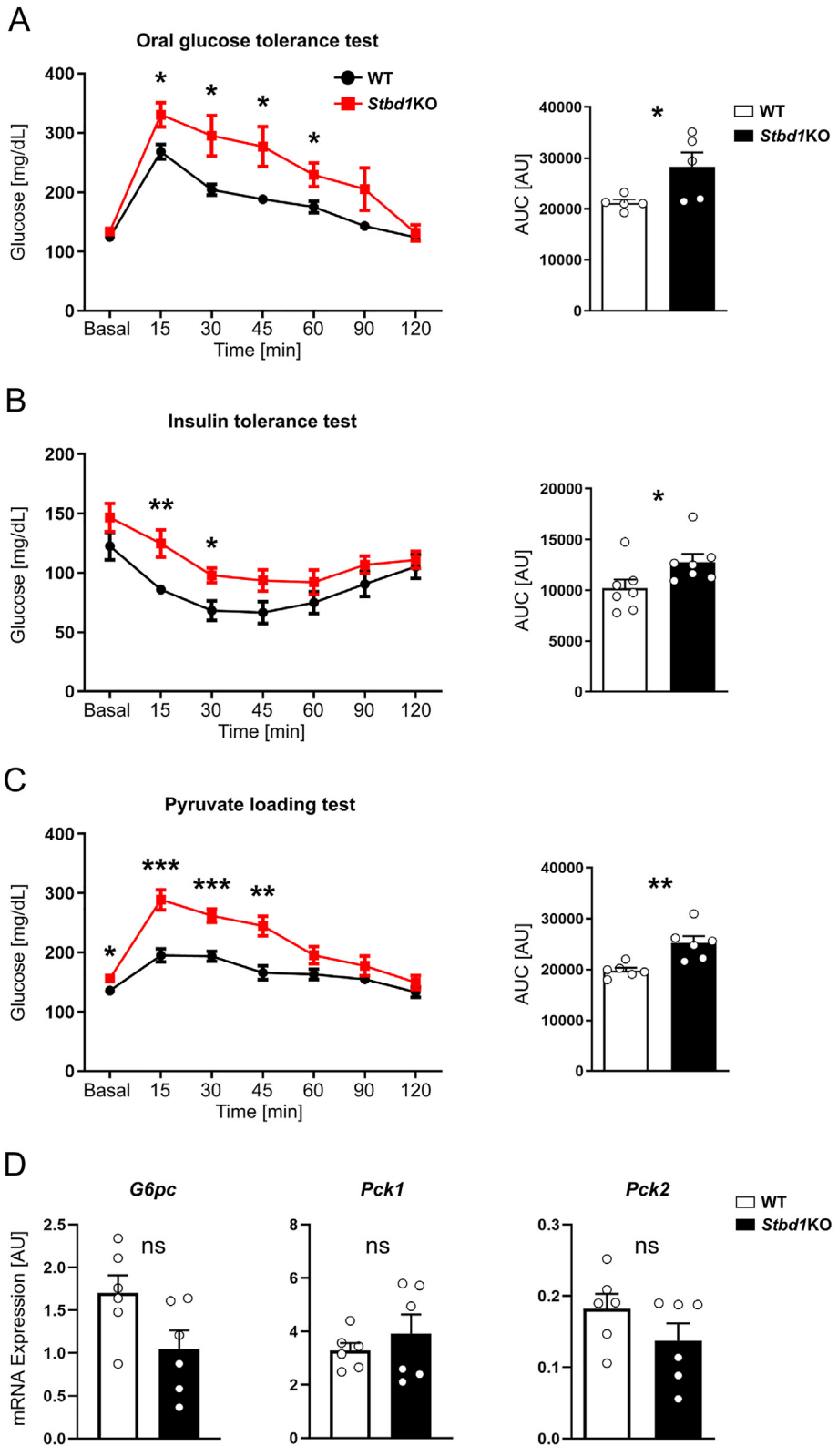

Fig. 2. Glucose, insulin and pyruvate loading tests
For the loading tests, blood glucose was measured in *Stbd1*KO and wild type mice prior to and at the indicated points following substance administration. The area under curve (AUC) was calculated and compared between the two genotypes. (A) Glucose tolerance test: A glucose bolus (2 g/kg BW) was orally administrated in 6-h fasted mice (n = 5 per genotype). (B) Insulin tolerance test: Insulin (0.75 units/kg BW) was intraperitoneally injected in mice fasted for 4 h (n = 7 per genotype), (C) Pyruvate loading test: 6-h fasted mice were intraperitoneally injected with pyruvate (2 g/kg BW) (n = 6 per genotype). (D) Expression levels of gluconeogenic genes (*G6pc*, *Pck1* and *Pck2*, encoding glucose-6-phosphatase, cytoplasmic- and mitochondrial phosphoenolpyruvate carboxykinase, respectively) in the liver of randomly fed wild type and *Stbd1*KO mice (n = 6 per genotype), relative to the expression levels of the β-actin gene, determined by quantitative PCR. Values are presented as mean ± SEM, *P < 0.05, **P < 0.01, ***P < 0.001 (unpaired Student's *t*-test). AU, arbitrary units; BW, body weight.

comparable blood glucose levels both at randomly fed conditions and following a 6-h fast (Fig. 1D). However, *Stbd1*-deficient animals exhibited reduced efficiency to defend blood glucose levels during an 18-h fast (Fig. 1D) which may correlate with the depletion of their hepatic glycogen stores (Fig. 1B). Interestingly, after 3 h of refeeding following an 18-h fast, blood glucose in *Stbd1*KO mice was found significantly increased as compared to controls which may suggest delayed glucose clearance from the blood (Fig. 1D). Moreover, upon a prolonged starvation of 36 h, blood glucose levels in *Stbd1*KO mice appeared significantly elevated as compared to those of control animals (Fig. 1D).

The reduced liver glycogen content and increased blood glucose levels during prolonged starvation and upon refeeding after fasting are compatible with a state of glucose intolerance and insulin resistance in *Stbd1*KO mice. To address the above, we initially evaluated the levels of serum insulin by means of ELISA. Following a 6-h morning fast, *Stbd1*KO mice featured significantly elevated blood insulin concentration as compared to controls whereas similarly increased insulin levels were measured in both genotypes after 1 h of refeeding following a 6-h fast (Fig. 1E).

To further support the above observations, we performed metabolic tests on *Stbd1*KO mice and control animals. *Stbd1*KO mice were found to exhibit reduced tolerance to orally administered glucose (Fig. 2A) and an attenuated response to the glucose-lowering effect of insulin (Fig. 2B). Furthermore, *Stbd1*-deficient mice featured increased glucose production in response to pyruvate loading suggesting enhanced gluconeogenesis (Fig. 2C). To gain insights into the underlying basis of increased hepatic glucose production in *Stbd1*KO mice, we evaluated the gene expression levels of two key gluconeogenic enzymes, glucose-6-phosphatase (G6PC) and phosphoenolpyruvate carboxykinase (PEPCK) in the liver of randomly fed mice. We observed no significant difference between wild type and *Stbd1*-deficient animals, suggesting that the increased gluconeogenesis rates in *Stbd1*KO mice are not associated with elevated expression of the above genes (Fig. 2D).

Binding of insulin to its cell surface receptor initiates a signaling cascade that results in the phosphorylation of downstream components. Among the downstream effectors of insulin signaling are the serine/threonine kinase AKT and the transcription factor FOXO1. The phosphorylation status of the above proteins is commonly assessed as a readout of insulin signaling. Following the intraperitoneal administration of an insulin bolus, phosphorylation of AKT (Ser^{473}) and FOXO1 (Ser^{256}) in both the liver and gastrocnemius muscle of *Stbd1*KO mice was significantly diminished as compared to controls, in agreement with an attenuated response of these tissues to insulin (Fig. 3A and B).

An additional pathological manifestation associated with insulin resistance is hepatic steatosis. Nevertheless, quantitative assessment of triglyceride levels in the liver revealed no significant difference between wild type and *Stbd1*KO animals both at fed and fasting conditions (Fig. 3C). The above results were in agreement with the qualitative evaluation of lipid deposition in the liver using Oil Red O staining on histological sections (Fig. 3D). To further assess potential perturbations in lipid homeostasis we measured the levels of diacylglycerols and sphingolipids in the liver of randomly fed *Stbd1*KO and wild type mice. While total hepatic diacylglycerol and ceramide content was comparable between both genotypes (Fig. 3E), *Stbd1*KO mice displayed increased total sphingomyelin levels, in particular saturated very long chain species (Fig. 3E and Fig. S2).

A major contributor to the development of insulin resistance is ER stress. It has been recently reported that STBD1 is a downstream target of the unfolded protein response (UPR) pathway and is required to promote glycogen clustering, associated with enhanced cell survival during ER stress in myoblasts [14]. Given the above correlation between STBD1 and ER stress, we evaluated the expression levels of different UPR marker genes in the liver of randomly fed *Stbd1*KO and control mice. We found no significant difference in the expression levels of *Bip*, *Atf4*, *Edem1*, spliced *Xbp1*, *Casp12* and *Chop* between the two genotypes suggesting that *Stbd1* inactivation does not lead to increased ER stress in the liver (Fig. 4).

3.3. Enhanced ER-mitochondria contact and altered mitochondrial morphology in the liver of Stbd1KO mice

Insulin resistance has been strongly associated with distortions in the structural and functional integrity of ER-mitochondria contact regions. Nevertheless, it is still controversial whether hepatic insulin resistance is related to enhanced or reduced ER-mitochondria association. Given that STBD1 has been reported to localize at MERCs, we evaluated morphometric parameters of ER-mitochondria contact and mitochondrial morphology in the liver of *Stbd1*KO and control mice by means of transmission electron microscopy. We found that the area of contact between the ER and mitochondria was increased in *Stbd1*KO mice (Fig. 5A and B). Furthermore, mitochondria appeared smaller and more circular in *Stbd1*KO animals, as evidenced by the quantitative assessment of mitochondrial perimeter, area, circularity and aspect ratio (Fig. 5B).

We further addressed the question of whether the enhanced ER-mitochondria contact area and the observed alterations in mitochondrial morphology in the liver of *Stbd1*KO mice affect mitochondrial function. For this, we evaluated the relative abundance of respiratory chain complexes in the liver by western blotting. We found a statistically significant reduction in complex I subunit NDUFB8 in *Stbd1*KO mice but no alterations in additional complexes (Fig. 6A). Nevertheless, the enzymatic activities of respiratory chain complexes were found to be comparable between both genotypes suggesting that STBD1 deficiency and the observed distortions in MERCs and mitochondrial dynamics are likely not associated with impaired mitochondrial function (Fig. 6B).

4. Discussion

STBD1 is an ER-resident, glycogen-binding protein of poorly characterized function. In the present study we have addressed the implication of STBD1 deficiency in insulin resistance in 24-week-old male mice. We provide evidence that *Stbd1*KO mice display reduced hepatic glycogen content and additional distortions in glucose metabolism, compatible with insulin resistance, including glucose intolerance, impaired insulin signaling and enhanced gluconeogenesis. The above metabolic abnormalities are associated with increased ER-mitochondria contact and morphological changes in mitochondria.

Our findings revealed reduced liver glycogen stores in *Stbd1*KO mice, under randomly fed conditions. Given that the glycogen content in skeletal muscle was comparable between *Stbd1*KO and wild type animals, the reduced hepatic glycogen levels in *Stbd1*-deficient mice could likely be secondary to insulin resistance and not to a primary effect of STBD1 deficiency on glycogen metabolism. The above is supported by our previously reported findings that neither the silencing nor overexpression of STBD1 in cultured cells influence total cellular glycogen levels [14]. In any case, the reduced amount of liver glycogen in *Stbd1*KO animals most likely underlies the near complete depletion of their hepatic glycogen stores after 18 h of fasting. This, on a background of insulin resistance, results in a pattern of decreased blood glucose at 18 h of fasting, whereas postprandially and after prolonged fasting blood glucose levels in *Stbd1*KO mice are significantly increased as compared to controls. Furthermore, *Stbd1*KO animals present with enhanced gluconeogenesis and attenuated insulin signaling in both

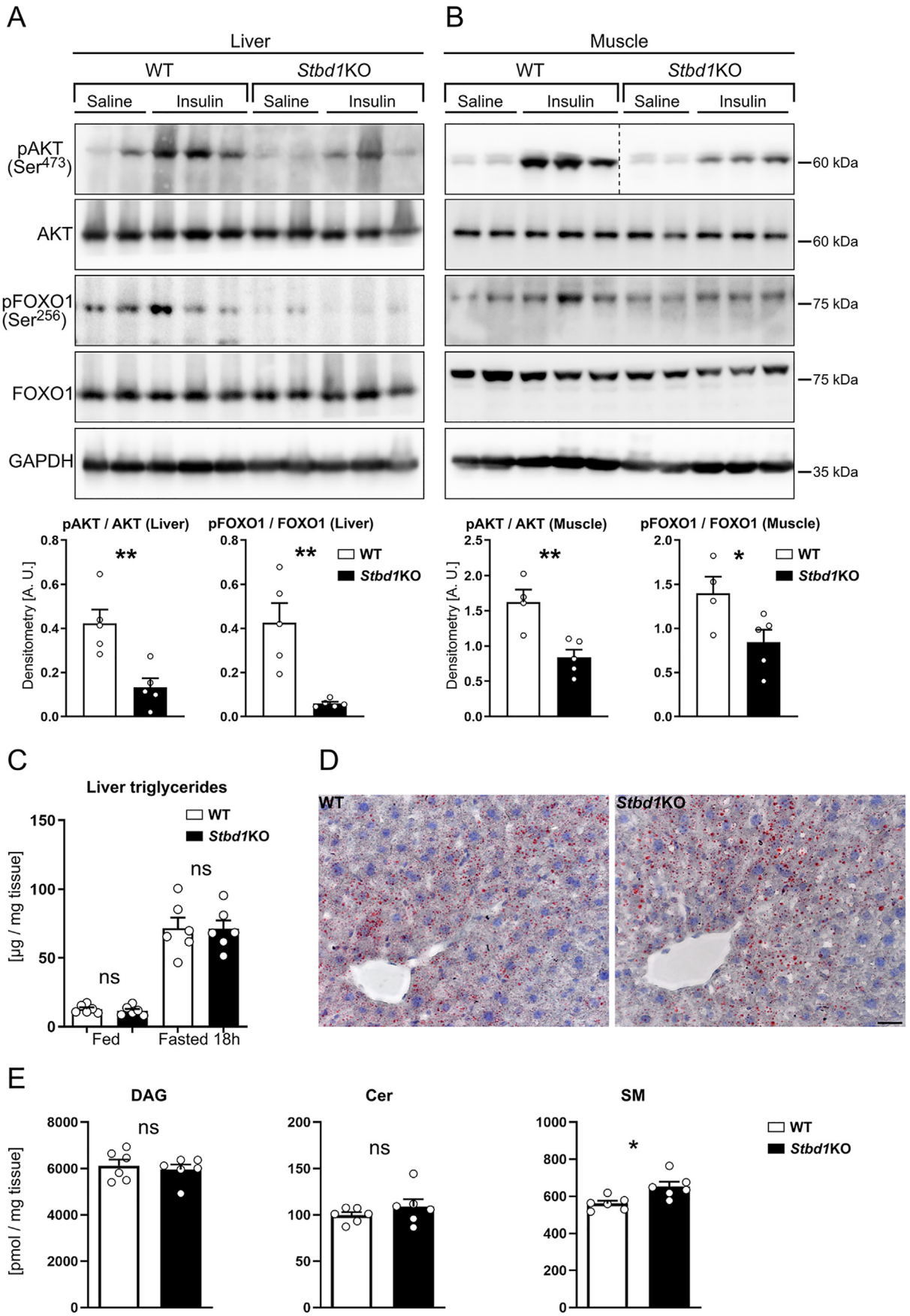
A
Liver
WT
Stbd1KO
Saline
Insulin
Saline
Insulin
pAKT (Ser473)
AKT
pFOXO1 (Ser256)
FOXO1
GAPDH
60 kDa
60 kDa
75 kDa
75 kDa
35 kDa
B
Muscle
WT
Stbd1KO
Saline
Insulin
Saline
Insulin
pAKT / AKT (Liver)
pFOXO1 / FOXO1 (Liver)
pAKT / AKT (Muscle)
pFOXO1 / FOXO1 (Muscle)
Densitometry [A. U.]
WT
Stbd1KO
C
Liver triglycerides
[µg / mg tissue]
ns
ns
Fed
Fasted 18h
D
WT
Stbd1KO
E
DAG
Cer
SM
[pmol / mg tissue]
ns
ns
*
WT
Stbd1KO

Fig. 3. *Stbd1*-deficient mice feature attenuated activation of insulin signaling in liver and muscle but no signs of hepatic steatosis
(A-B) Representative western blot and densitometry for the assessment of insulin induced AKT (Ser^{473}) and FOXO1 (Ser^{256}) phosphorylation in the liver (A) and the gastrocnemius muscle (B), of mice intraperitoneally injected with either insulin (2 units/kg BW) or saline. The dashed line in (B) refers to the splicing of the western blot image following the removal of irrelevant lanes. The ratios of phosphorylated AKT (Ser^{473}) and FOXO1 (Ser^{256}) to total AKT and FOXO1 levels respectively, were determined using densitometry (liver, n = 5 per genotype; muscle, n = 4 for wild type, n = 5 for *Stbd1*KO). GAPDH was used as loading control. (C) Assessment of liver triglyceride content in randomly fed and 18 h-fasted mice (n = 6 per group). (D) Qualitative assessment of lipid deposition by Oil Red O staining on liver cryosections. Nuclei were counterstained with hematoxylin. (E) Quantitative determination of the levels of total diacylglycerols (DAG), ceramides (Cer) and sphingomyelins (SM) in the liver of randomly fed *Stbd1*KO and wild type mice (n = 6 per genotype). Values are expressed as mean ± SEM, *P < 0.05, **P < 0.01, ns, not significant (unpaired Student's *t*-test). AU, arbitrary units; BW, body weight. Scale bar, 25 μm.

the liver and skeletal muscle. The above findings suggest increased liver glucose output and impaired glucose uptake by peripheral tissues which may explain the elevated blood glucose levels post-prandially and following prolonged fasting. Failure of insulin to suppress hepatic gluconeogenesis contributes to enhanced glucose production in insulin resistance states. However, expression levels of the gluconeogenic enzymes G6PC and PEPCK were not found elevated in *Stbd1*KO mice. Hyperglycemia and hyperinsulinemia are not necessarily associated with increased expression levels of G6PC and PEPCK. This has been reported for both rodent models of fasting hyperglycemia and patients with T2D [26]. Furthermore, the transcription of the above gluconeogenic genes is regulated by multiple transcription factors. The lack of increased expression levels of G6PC and PEPCK in the presence of enhanced hepatic glucose production in *Stbd1*KO mice could therefore also be ascribed to the complexity of the transcriptional regulation of the corresponding genes.

Cumulative evidence strongly supports the importance of the structural integrity of MERCs in the regulation of insulin signaling and the development of hepatic insulin resistance [27,28]. Nevertheless, the precise involvement of ER-mitochondria cross-talk in the response of tissues to insulin remains unclear. This is primarily due to contradictory findings with regards to whether insulin resistance is associated with disrupted or enhanced ER-mitochondria communication. In particular, the structural integrity of MERCs was found to be impaired in the liver of both genetically engineered and diet-induced obese mice [29]. However, the above association between impaired ER-mitochondria cross-talk and insulin resistance was challenged by a study reporting enhanced ER-mitochondria communication in the liver of obese mice and an improvement of insulin response upon reduction of MERCs [30]. Importantly, the correlation between the structural integrity of MERCs and insulin resistance appears to be reciprocal which further adds to the complexity of their cause-and-effect relationship [10]. Our findings indicate increased contact area between the ER and mitochondria in *Stbd1*KO mice and are therefore in support of the notion that insulin resistance is associated with enhanced ER-mitochondria cross-talk.

MERCs have been recognized as important mediators of mitochondrial dynamics which mainly describes the processes of

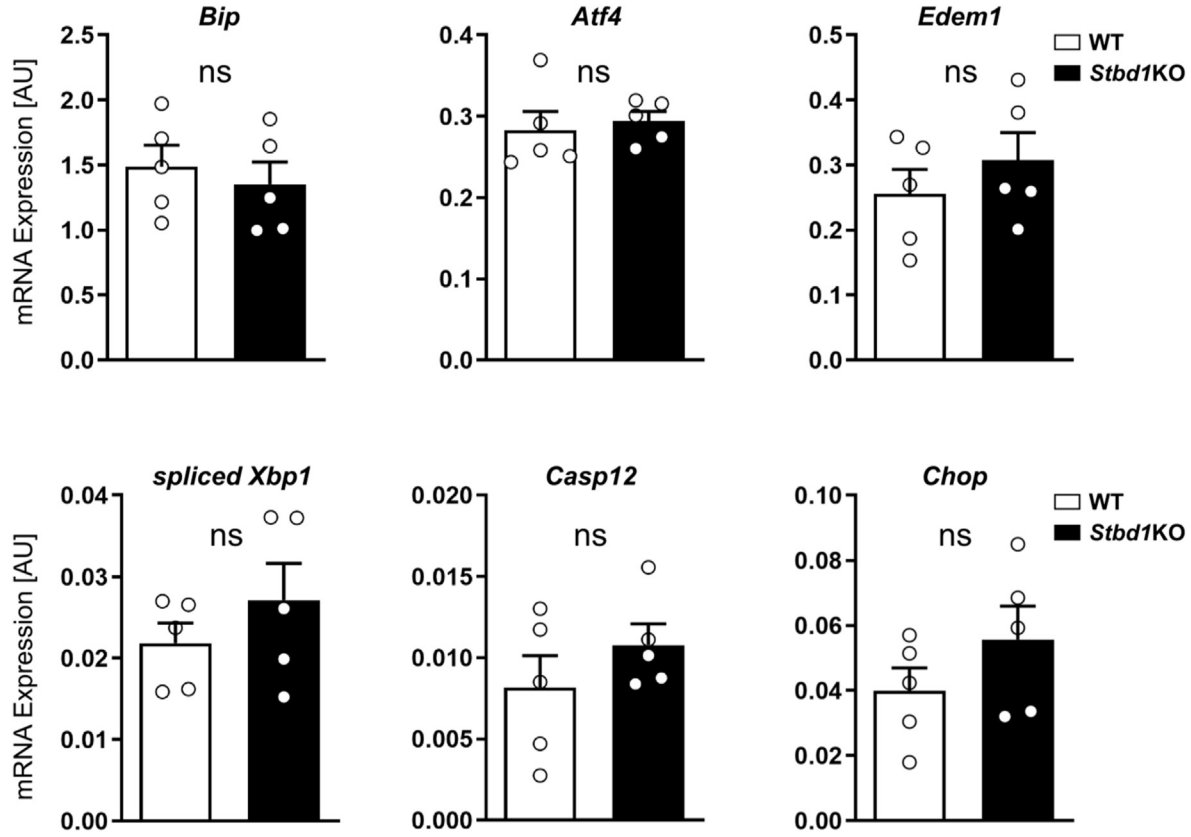

Fig. 4. STBD1 deficiency does not cause ER stress in the liver
The expression levels of representative markers of the unfolded protein response pathway were determined in the liver of randomly fed *Stbd1*KO and wild type mice (n = 5 per genotype) by quantitative PCR. The values were normalized to the expression of β-actin. Values are expressed as mean ± SEM, ns, not significant, (unpaired Student's *t*-test), AU, arbitrary units.

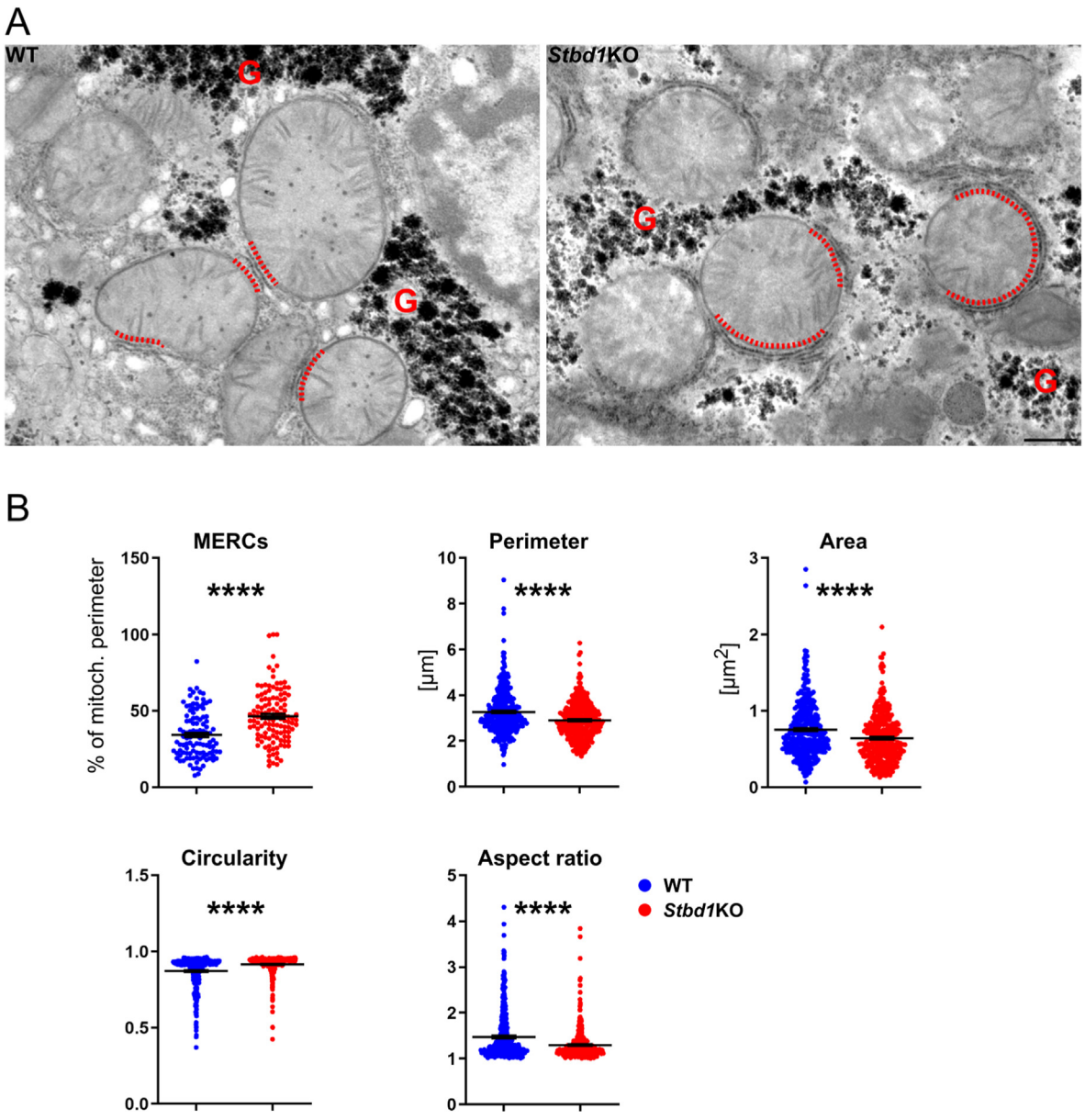

Fig. 5. STBD1 deficiency is associated with increased mitochondria-ER contact sites and altered mitochondrial morphology in the liver
(A) Representative transmission electron micrographs of liver mitochondria of randomly fed *Stbd1*KO and wild type mice. The regions of contact between mitochondria and the ER (MERCs) are indicated by red dashed lines. Note the reduced glycogen content in the liver of *Stbd1*KO mice. (B) Quantitative assessment of MERCs and mitochondrial morphological parameters. MERCs were quantitatively assessed by measuring the length of the mitochondrial interface in close apposition to the ER, expressed as a percentage of the mitochondrial perimeter (Wild type, n = 108; *Stbd1*KO, n = 123 mitochondria; 3 animals per genotype). Mitochondrial morphology was evaluated following the quantitative assessment of mitochondrial perimeter, area, circularity and aspect ratio using ImageJ (Wild type, n = 345; *Stbd1*KO, n = 348 mitochondria; 3 animals per genotype). G, glycogen. Values are expressed as mean ± SEM, ****P < 0.0001 (unpaired Student's *t*-test). Scale bar, 0.5 µm.

mitochondrial fusion and fission [31]. In particular, the contact regions between the ER and mitochondria were shown to define the sites of mitochondrial fission [32]. According to the above, an increase in MERCs is expected to shift the equilibrium between mitochondrial fusion and fission towards mitochondrial fragmentation. Several lines of evidence, support that insulin resistance and related metabolic conditions such as obesity and T2D are associated with increased mitochondrial fission. Hyperglycemia was reported to induce mitochondrial fragmentation in cultured myoblasts and hepatocytes [33]. In addition, mitochondria from T2D patients were found to be smaller in the skeletal muscle [34] and fragmented in the myocardium [35], as compared to those of healthy individuals. Conversely, insulin was shown to promote mitochondrial fusion in cultured cardiomyocytes [36]. In agreement with the published data, our results indicate that liver mitochondria in *Stbd1*KO mice are smaller and display increased circularity suggesting fragmentation of the mitochondrial network.

ER stress and mitochondrial dysfunction are major features of the molecular pathology of obesity and T2D in which insulin resistance is a common metabolic abnormality. Nevertheless, assessment of the levels of ER stress markers did not reveal any overt differences between *Stbd1*KO and control mice. Moreover, both genotypes displayed comparable enzymatic activity of respiratory chain complexes despite a statistically significant decrease in complex I abundance in *Stbd1*KO mice. The above findings may correlate with the fact that insulin resistance in *Stbd1*KO mice is not

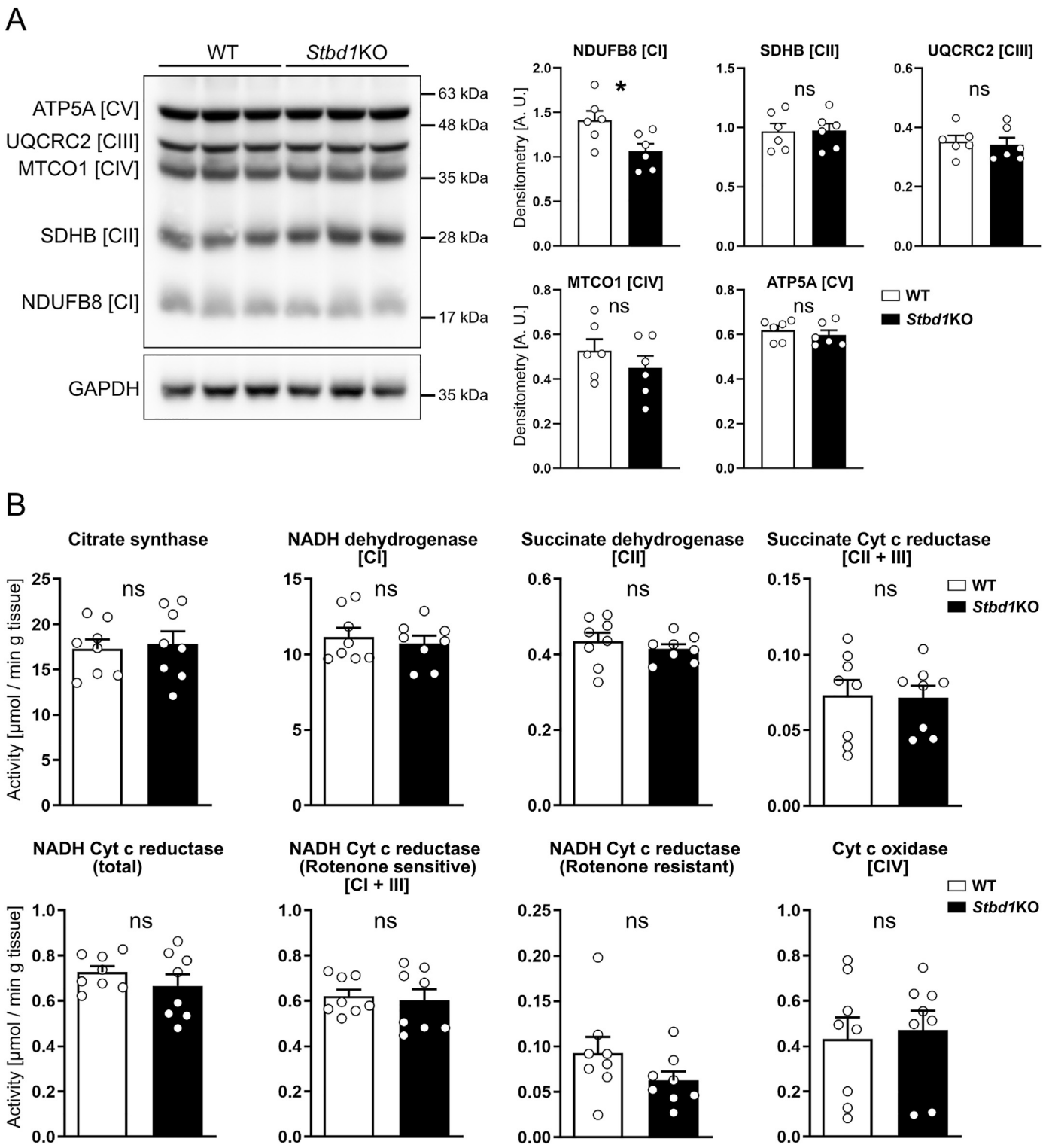

Fig. 6. *Stbd1*KO mice exhibit normal enzymatic activity of mitochondrial respiratory chain complexes in the liver
(A) Representative western blot and densitometry for the evaluation of the relative abundance of mitochondrial respiratory chain complexes (CI – CV) in the liver of randomly fed wild type and *Stbd1*KO mice. Densitometry analysis is presented as the ratio to GAPDH (n = 6 per genotype). (B) Assessment of the enzymatic activity of respiratory chain complexes (CI – CIV) in the liver of randomly fed wild type and *Stbd1*KO animals (n = 8 per genotype). Values are expressed as mean ± SEM, *P < 0.05, ns, not significant (unpaired Student's *t*-test).

associated with obesity, liver steatosis or profound hyperglycemia which could suggest an overall mild pathology. The lack of an elevation in hepatic triglycerides in the presence of hyperglycemia and hyperinsulinemia has been previously reported in mice with liver specific inactivation of the insulin receptor (LIRKO) [37]. Despite hyperinsulinemia and hyperglycemia these mice display

normal body weight and liver triglyceride levels in contrast to insulin resistant mouse models of T2D such as high fat diet-fed or *ob*/*ob* mice which exhibit both hyperglycemia and hypertriglyceridemia. The origin for this discrepancy lies in the concept of selective resistance in the inhibitory effect of insulin on the process of hepatic gluconeogenesis, whereas stimulation of lipogenesis remains insulin sensitive [38]. On the other hand, insulin resistance in both pathways results in the manifestation of hyperglycemia in the absence of elevated triglycerides, as reported for LIRKO animals. A similar total insulin resistance in the liver of *Stbd1*-deficient mice would be in agreement with the herein observed increased gluconeogenesis and normal hepatic triglyceride levels. Similar to triglycerides, *Stbd1*-deficient mice displayed normal levels of liver diacylglycerol and ceramide lipids. However, hepatic sphingomyelins appeared mildly but significantly elevated in *Stbd1*KO mice. This may suggest that sphingomyelin levels could be a more sensitive indicator of insulin resistance. Alternatively, the increased levels of liver sphingomyelins in *Stbd1*KO mice could be related to the herein reported structural alterations in ER-mitochondria contacts since MERCs are major sites of sphingolipid metabolism [39].

In conclusion, the data presented in this study identify STBD1 deficiency as a susceptibility factor for insulin resistance. The herein reported distortions in insulin signaling are associated with enhanced ER-mitochondria association in the liver and may be related to the previously reported localization of STBD1 at MERCs.

Funding and additional information

This work was supported by the European Regional Development Fund and the Republic of Cyprus through the Research and Innovation Foundation (Project: POST-DOC/0718/0125). We thank Daniel Herrmann for excellent technical assistance with the LC-MS/MS analyses.

Author contributions

S.K.: Investigation, Data curation, Formal analysis, Writing-Original Draft; A.T.: Investigation, Formal analysis; L.P.: Investigation; F. S.: Investigation, Formal analysis; M.Z.: Formal analysis; R.P.: Investigation; B.K.: Resources; M.I.P.: Resources, Writing-Review & Editing; A.D.: Resources, Writing-Review & Editing; P.P.P.: Conceptualization, Methodology, Formal analysis, Project administration, Funding acquisition.

Declaration of competing interest

The authors declare that they have no competing interests.

Appendix A. Supplementary data

Supplementary data to this article can be found online at https://doi.org/10.1016/j.biochi.2022.06.003.

References

[1] M.C. Petersen, G.I. Shulman, Mechanisms of insulin action and insulin resistance, Physiol. Rev. 98 (2018) 2133–2223.
[2] S.E. Kahn, The relative contributions of insulin resistance and beta-cell dysfunction to the pathophysiology of Type 2 diabetes, Diabetologia 46 (2003) 3–19.
[3] R.A. Scott, V. Lagou, R.P. Welch, E. Wheeler, M.E. Montasser, J. Luan, R. Magi, R.J. Strawbridge, E. Rehnberg, S. Gustafsson, S. Kanoni, L.J. Rasmussen-Torvik, L. Yengo, C. Lecoeur, D. Shungin, S. Sanna, C. Sidore, P.C. Johnson, J.W. Jukema, T. Johnson, A. Mahajan, N. Verweij, G. Thorleifsson, J.J. Hottenga, S. Shah, A.V. Smith, B. Sennblad, C. Gieger, P. Salo, M. Perola, N.J. Timpson, D.M. Evans, B.S. Pourcain, Y. Wu, J.S. Andrews, J. Hui, L.F. Bielak, W. Zhao, M. Horikoshi, P. Navarro, A. Isaacs, J.R. O'Connell, K. Stirrups, V. Vitart, C. Hayward, T. Esko, E. Mihailov, R.M. Fraser, T. Fall, B.F. Voight, S. Raychaudhuri, H. Chen, C.M. Lindgren, A.P. Morris, N.W. Rayner, N. Robertson, D. Rybin, C.T. Liu, J.S. Beckmann, S.M. Willems, P.S. Chines, A.U. Jackson, H.M. Kang, H.M. Stringham, K. Song, T. Tanaka, J.F. Peden, A. Goel, A.A. Hicks, P. An, M. Muller-Nurasyid, A. Franco-Cereceda, L. Folkersen, L. Marullo, H. Jansen, A.J. Oldehinkel, M. Bruinenberg, J.S. Pankow, K.E. North, N.G. Forouhi, R.J. Loos, S. Edkins, T.V. Varga, G. Hallmans, H. Oksa, M. Antonella, R. Nagaraja, S. Trompet, I. Ford, S.J. Bakker, A. Kong, M. Kumari, B. Gigante, C. Herder, P.B. Munroe, M. Caulfield, J. Antti, M. Mangino, K. Small, I. Miljkovic, Y. Liu, M. Atalay, W. Kiess, A.L. James, F. Rivadeneira, A.G. Uitterlinden, C.N. Palmer, A.S. Doney, G. Willemsen, J.H. Smit, S. Campbell, O. Polasek, L.L. Bonnycastle, S. Hercberg, M. Dimitriou, J.L. Bolton, G.R. Fowkes, P. Kovacs, J. Lindstrom, T. Zemunik, S. Bandinelli, S.H. Wild, H.V. Basart, W. Rathmann, H. Grallert, D.I.G. Replication, C. Meta-analysis, W. Maerz, M.E. Kleber, B.O. Boehm, A. Peters, P.P. Pramstaller, M.A. Province, I.B. Borecki, N.D. Hastie, I. Rudan, H. Campbell, H. Watkins, M. Farrall, M. Stumvoll, L. Ferrucci, D.M. Waterworth, R.N. Bergman, F.S. Collins, J. Tuomilehto, R.M. Watanabe, E.J. de Geus, B.W. Penninx, A. Hofman, B.A. Oostra, B.M. Psaty, P. Vollenweider, J.F. Wilson, A.F. Wright, G.K. Hovingh, A. Metspalu, M. Uusitupa, P.K. Magnusson, K.O. Kyvik, J. Kaprio, J.F. Price, G.V. Dedoussis, P. Deloukas, P. Meneton, L. Lind, M. Boehnke, A.R. Shuldiner, C.M. van Duijn, A.D. Morris, A. Toenjes, P.A. Peyser, J.P. Beilby, A. Korner, J. Kuusisto, M. Laakso, S.R. Bornstein, P.E. Schwarz, T.A. Lakka, R. Rauramaa, L.S. Adair, G.D. Smith, T.D. Spector, T. Illig, U. de Faire, A. Hamsten, V. Gudnason, M. Kivimaki, A. Hingorani, S.M. Keinanen-Kiukaanniemi, T.E. Saaristo, D.I. Boomsma, K. Stefansson, P. van der Harst, J. Dupuis, N.L. Pedersen, N. Sattar, T.B. Harris, F. Cucca, S. Ripatti, V. Salomaa, K.L. Mohlke, B. Balkau, P. Froguel, A. Pouta, M.R. Jarvelin, N.J. Wareham, N. Bouatia-Naji, M.I. McCarthy, P.W. Franks, J.B. Meigs, T.M. Teslovich, J.C. Florez, C. Langenberg, E. Ingelsson, I. Prokopenko, I. Barroso, Large-scale association analyses identify new loci influencing glycemic traits and provide insight into the underlying biological pathways, Nat. Genet. 44 (2012) 991–1005.
[4] W. Zhao, A. Rasheed, E. Tikkanen, J.J. Lee, A.S. Butterworth, J.M.M. Howson, T.L. Assimes, R. Chowdhury, M. Orho-Melander, S. Damrauer, A. Small, S. Asma, M. Imamura, T. Yamauch, J.C. Chambers, P. Chen, B.R. Sapkota, N. Shah, S. Jabeen, P. Surendran, Y. Lu, W. Zhang, A. Imran, S. Abbas, F. Majeed, K. Trindade, N. Qamar, N.H. Mallick, Z. Yaqoob, T. Saghir, S.N.H. Rizvi, A. Memon, S.Z. Rasheed, F.U. Memon, K. Mehmood, N. Ahmed, I.H. Qureshi, S. Tanveer Us, W. Iqbal, U. Malik, N. Mehra, J.Z. Kuo, W.H. Sheu, X. Guo, C.A. Hsiung, J.J. Juang, K.D. Taylor, Y.J. Hung, W.J. Lee, T. Quertermous, I.T. Lee, C.C. Hsu, E.P. Bottinger, S. Ralhan, Y.Y. Teo, T.D. Wang, D.S. Alam, E. Di Angelantonio, S. Epstein, S.F. Nielsen, B.G. Nordestgaard, A. Tybjaerg-Hansen, R. Young, C.H.D.E. Consortium, M. Benn, R. Frikke-Schmidt, P.R. Kamstrup, E.-C. Consortium, E.P.-I. Consortium, B. Michigan, J.W. Jukema, N. Sattar, R. Smit, R.H. Chung, K.W. Liang, S. Anand, D.K. Sanghera, S. Ripatti, R.J.F. Loos, J.S. Kooner, E.S. Tai, J.I. Rotter, Y.I. Chen, P. Frossard, S. Maeda, T. Kadowaki, M. Reilly, G. Pare, O. Melander, V. Salomaa, D.J. Rader, J. Danesh, B.F. Voight, D. Saleheen, Identification of new susceptibility loci for type 2 diabetes and shared etiological pathways with coronary heart disease, Nat. Genet. 49 (2017) 1450–1457.
[5] S.P. Sah, B. Singh, S. Choudhary, A. Kumar, Animal models of insulin resistance: a review, Pharmacol. Rep. 68 (2016) 1165–1177.
[6] C. Lopez-Crisosto, R. Bravo-Sagua, M. Rodriguez-Pena, C. Mera, P.F. Castro, A.F. Quest, B.A. Rothermel, M. Cifuentes, S. Lavandero, ER-to-mitochondria miscommunication and metabolic diseases, Biochim. Biophys. Acta 1852 (2015) 2096–2105.
[7] I. Gordaliza-Alaguero, C. Canto, A. Zorzano, Metabolic implications of organelle-mitochondria communication, EMBO Rep. 20 (2019), e47928.
[8] O. Moltedo, P. Remondelli, G. Amodio, The mitochondria-endoplasmic reticulum contacts and their critical role in aging and age-associated diseases, Front. Cell Dev. Biol. 7 (2019) 172.
[9] J. Rieusset, The role of endoplasmic reticulum-mitochondria contact sites in the control of glucose homeostasis: an update, Cell Death Dis. 9 (2018) 388.
[10] C. Betz, D. Stracka, C. Prescianotto-Baschong, M. Frieden, N. Demaurex, M.N. Hall, Feature Article: mTOR complex 2-Akt signaling at mitochondria-associated endoplasmic reticulum membranes (MAM) regulates mitochondrial physiology, Proc. Natl. Acad. Sci. U. S. A 110 (2013) 12526–12534.
[11] A. Demetriadou, J. Morales-Sanfrutos, M. Nearchou, O. Baba, K. Kyriacou, E.W. Tate, A. Drousiotou, P.P. Petrou, Mouse Stbd1 is N-myristoylated and affects ER-mitochondria association and mitochondrial morphology, J. Cell Sci. 130 (2017) 903–915.
[12] C.N. Poston, S.C. Krishnan, C.R. Bazemore-Walker, In-depth proteomic analysis of mammalian mitochondria-associated membranes (MAM), J. Proteonomics 79 (2013) 219–230.
[13] Z. Liu, X. Du, J. Deng, M. Gu, H. Hu, M. Gui, C.C. Yin, Z. Chang, The interactions between mitochondria and sarcoplasmic reticulum and the proteome characterization of mitochondrion-associated membrane from rabbit skeletal muscle, Proteomics 15 (2015) 2701–2704.
[14] A.A. Lytridou, A. Demetriadou, M. Christou, L. Potamiti, N.P. Mastroyiannopoulos, K. Kyriacou, L.A. Phylactou, A. Drousiotou, P.P. Petrou, Stbd1 promotes glycogen clustering during endoplasmic reticulum stress and supports survival of mouse myoblasts, J. Cell Sci. 133 (2020).
[15] A. Bradley, K. Anastassiadis, A. Ayadi, J.F. Battey, C. Bell, M.C. Birling, J. Bottomley, S.D. Brown, A. Burger, C.J. Bult, W. Bushell, F.S. Collins,

C. Desaintes, B. Doe, A. Economides, J.T. Eppig, R.H. Finnell, C. Fletcher, M. Fray, D. Frendewey, R.H. Friedel, F.G. Grosveld, J. Hansen, Y. Herault, G. Hicks, A. Horlein, R. Houghton, M. Hrabe de Angelis, D. Huylebroeck, V. Iyer, P.J. de Jong, J.A. Kadin, C. Kaloff, K. Kennedy, M. Koutsourakis, K.C. Lloyd, S. Marschall, J. Mason, C. McKerlie, M.P. McLeod, H. von Melchner, M. Moore, A.O. Mujica, A. Nagy, M. Nefedov, L.M. Nutter, G. Pavlovic, J.L. Peterson, J. Pollock, R. Ramirez-Solis, D.E. Rancourt, M. Raspa, J.E. Remacle, M. Ringwald, B. Rosen, N. Rosenthal, J. Rossant, P. Ruiz Noppinger, E. Ryder, J.Z. Schick, F. Schnutgen, P. Schofield, C. Seisenberger, M. Selloum, E.M. Simpson, W.C. Skarnes, D. Smedley, W.L. Stanford, A.F. Stewart, K. Stone, K. Swan, H. Tadepally, L. Teboul, G.P. Tocchini-Valentini, D. Valenzuela, A.P. West, K. Yamamura, Y. Yoshinaga, W. Wurst, The mammalian gene function resource: the International Knockout Mouse Consortium, Mamm. Genome 23 (2012) 580–586.

[16] H. Jouihan, Measurement of liver triglyceride content, Bio-protocol 2 (2012) e223.

[17] S. Zeitler, F. Schumacher, J. Monti, D. Anni, D. Guhathakurta, B. Kleuser, K. Friedland, A. Fejtova, J. Kornhuber, C. Rhein, Acid sphingomyelinase impacts canonical transient receptor potential channels 6 (TRPC6) activity in primary neuronal systems, Cells (2020) 9.

[18] A. Gulbins, F. Schumacher, K.A. Becker, B. Wilker, M. Soddemann, F. Boldrin, C.P. Muller, M.J. Edwards, M. Goodman, C.C. Caldwell, B. Kleuser, J. Kornhuber, I. Szabo, E. Gulbins, Antidepressants act by inducing autophagy controlled by sphingomyelin-ceramide, Mol. Psychiatr. 23 (2018) 2324–2346.

[19] E. Naser, S. Kadow, F. Schumacher, Z.H. Mohamed, C. Kappe, G. Hessler, B. Pollmeier, B. Kleuser, C. Arenz, K.A. Becker, E. Gulbins, A. Carpinteiro, Characterization of the small molecule ARC39, a direct and specific inhibitor of acid sphingomyelinase in vitro, J. Lipid Res. 61 (2020) 896–910.

[20] P.K. Smith, R.I. Krohn, G.T. Hermanson, A.K. Mallia, F.H. Gartner, M.D. Provenzano, E.K. Fujimoto, N.M. Goeke, B.J. Olson, D.C. Klenk, Measurement of protein using bicinchoninic acid, Anal. Biochem. 150 (1985) 76–85.

[21] J. Lam, P. Katti, M. Biete, M. Mungai, S. AshShareef, K. Neikirk, E. Garza Lopez, Z. Vue, T.A. Christensen, H.K. Beasley, T.A. Rodman, S.A. Murray, J.L. Salisbury, B. Glancy, J. Shao, R.O. Pereira, E.D. Abel, A. Hinton Jr., A universal approach to analyzing transmission electron microscopy with ImageJ, Cells (2021) 10.

[22] R. Van Coster, A. Lombres, D.C. De Vivo, T.L. Chi, W.E. Dodson, S. Rothman, E.J. Orrechio, W. Grover, G.T. Berry, J.F. Schwartz, et al., Cytochrome c oxidase-associated Leigh syndrome: phenotypic features and pathogenetic speculations, J. Neurol. Sci. 104 (1991) 97–111.

[23] J.M. Ruijter, C. Ramakers, W.M. Hoogaars, Y. Karlen, O. Bakker, M.J. van den Hoff, A.F. Moorman, Amplification efficiency: linking baseline and bias in the analysis of quantitative PCR data, Nucleic Acids Res. 37 (2009) e45.

[24] S. Jiang, B. Heller, V.S. Tagliabracci, L. Zhai, J.M. Irimia, A.A. DePaoli-Roach, C.D. Wells, A.V. Skurat, P.J. Roach, Starch binding domain-containing protein 1/genethonin 1 is a novel participant in glycogen metabolism, J. Biol. Chem. 285 (2010) 34960–34971.

[25] Y. Zhu, M. Zhang, A.R. Kelly, A. Cheng, The carbohydrate-binding domain of overexpressed STBD1 is important for its stability and protein-protein interactions, Biosci. Rep. 34 (2014).

[26] V.T. Samuel, S.A. Beddow, T. Iwasaki, X.M. Zhang, X. Chu, C.D. Still, G.S. Gerhard, G.I. Shulman, Fasting hyperglycemia is not associated with increased expression of PEPCK or G6Pc in patients with Type 2 Diabetes, Proc. Natl. Acad. Sci. U. S. A 106 (2009) 12121–12126.

[27] H. Cheng, X. Gang, G. He, Y. Liu, Y. Wang, X. Zhao, G. Wang, The molecular mechanisms underlying mitochondria-associated endoplasmic reticulum membrane-induced insulin resistance, Front. Endocrinol. 11 (2020), 592129.

[28] L.K. Townsend, H.S. Brunetta, M.A.S. Mori, Mitochondria-associated ER membranes in glucose homeostasis and insulin resistance, Am. J. Physiol. Endocrinol. Metab. 319 (2020) E1053–E1060.

[29] E. Tubbs, P. Theurey, G. Vial, N. Bendridi, A. Bravard, M.A. Chauvin, J. Ji-Cao, F. Zoulim, B. Bartosch, M. Ovize, H. Vidal, J. Rieusset, Mitochondria-associated endoplasmic reticulum membrane (MAM) integrity is required for insulin signaling and is implicated in hepatic insulin resistance, Diabetes 63 (2014) 3279–3294.

[30] A.P. Arruda, B.M. Pers, G. Parlakgul, E. Guney, K. Inouye, G.S. Hotamisligil, Chronic enrichment of hepatic endoplasmic reticulum-mitochondria contact leads to mitochondrial dysfunction in obesity, Nat. Med. 20 (2014) 1427–1435.

[31] S. Kyriakoudi, A. Drousiotou, P.P. Petrou, When the balance tips: dysregulation of mitochondrial dynamics as a culprit in disease, Int. J. Mol. Sci. 22 (2021).

[32] J.R. Friedman, L.L. Lackner, M. West, J.R. DiBenedetto, J. Nunnari, G.K. Voeltz, ER tubules mark sites of mitochondrial division, Science 334 (2011) 358–362.

[33] T. Yu, J.L. Robotham, Y. Yoon, Increased production of reactive oxygen species in hyperglycemic conditions requires dynamic change of mitochondrial morphology, Proc. Natl. Acad. Sci. U. S. A 103 (2006) 2653–2658.

[34] D.E. Kelley, J. He, E.V. Menshikova, V.B. Ritov, Dysfunction of mitochondria in human skeletal muscle in type 2 diabetes, Diabetes 51 (2002) 2944–2950.

[35] D. Montaigne, X. Marechal, A. Coisne, N. Debry, T. Modine, G. Fayad, C. Potelle, J.M. El Arid, S. Mouton, Y. Sebti, H. Duez, S. Preau, I. Remy-Jouet, F. Zerimech, M. Koussa, V. Richard, R. Neviere, J.L. Edme, P. Lefebvre, B. Staels, Myocardial contractile dysfunction is associated with impaired mitochondrial function and dynamics in type 2 diabetic but not in obese patients, Circulation 130 (2014) 554–564.

[36] V. Parra, H.E. Verdejo, M. Iglewski, A. Del Campo, R. Troncoso, D. Jones, Y. Zhu, J. Kuzmicic, C. Pennanen, C. Lopez-Crisosto, F. Jana, J. Ferreira, E. Noguera, M. Chiong, D.A. Bernlohr, A. Klip, J.A. Hill, B.A. Rothermel, E.D. Abel, A. Zorzano, S. Lavandero, Insulin stimulates mitochondrial fusion and function in cardiomyocytes via the Akt-mTOR-NFkappaB-Opa-1 signaling pathway, Diabetes 63 (2014) 75–88.

[37] S.B. Biddinger, A. Hernandez-Ono, C. Rask-Madsen, J.T. Haas, J.O. Aleman, R. Suzuki, E.F. Scapa, C. Agarwal, M.C. Carey, G. Stephanopoulos, D.E. Cohen, G.L. King, H.N. Ginsberg, C.R. Kahn, Hepatic insulin resistance is sufficient to produce dyslipidemia and susceptibility to atherosclerosis, Cell Metabol. 7 (2008) 125–134.

[38] M.S. Brown, J.L. Goldstein, Selective versus total insulin resistance: a pathogenic paradox, Cell Metabol. 7 (2008) 95–96.

[39] K. Roszczyc-Owsiejczuk, P. Zabielski, Sphingolipids as a culprit of mitochondrial dysfunction in insulin resistance and type 2 diabetes, Front. Endocrinol. 12 (2021), 635175.